

# A RAPID X-RAY FLARE IN THE RADIO-LOUD NARROW LINE QUASAR PKS 0558-504

T.G. WANG<sup>1</sup>, M. MATSUOKA<sup>2</sup>, H. KUBO<sup>3</sup>, T. MIHARA<sup>4</sup>, H. NEGORO<sup>4</sup>

*Draft version October 24, 2018*

## ABSTRACT

We report the detection of a very short time scale flare in the radio-loud narrow line quasars PKS 0558-504 by using ASCA. The X-ray count rates increased and decreased by a factor of two in 33 minutes, and possibly by 40% in as short as two minutes during this flare, confirming that such flare event does occur in this object with imaging detectors. The implied largest rate of change in luminosity in 0.8-10 keV alone,  $dL/dt \simeq (1.8 \pm 0.4) 10^{42} \text{ ergs s}^{-2}$ , is several times higher than the limit sets for the isotropic emitting plasma around a Kerr black hole. Either emission from a relativistic boosting jet or a magnetic heated corona may explain such high radiative efficiency. Magnetic field with a strength of at least a few  $10^4$  Gauss is required in the latter case. The spectrum during this flare is significant harder than the average one. Three radio loud narrow line active galactic nuclei (AGN) possess considerably smaller black holes than in radio loud AGN in bright quasar survey, indicating they are still in a phase of the rapid growth of the black hole by accretion.

*Subject headings:* Galaxies: active–Seyfert–Quasars: individual(PKS 0558-504) –Radiation: X-Ray – Black Hole

## 1. INTRODUCTION

Most Active Galactic Nuclei (AGN) show some variations in fluxes. The timescale and amplitude depends strongly on the wavelength observed: particularly, the amplitude is larger and time scale shorter in the X-ray band than in the optical one. Large amplitude variations over a time scale from minutes to hours have been reported for Seyfert galaxies and a particular beamed class of AGN named blazars (e.g., Barr & Mushotzky 1986, McHardy 1989, Catanese & Sambrana 2000). A physical causality argument leads to either very small size of the emission region and/or relativistic beaming in these objects. In fact, combining with the large energy output in the X-ray band, this is considered one strong evidence for their extremely high radiative efficiency, which leads to the general picture of massive black hole accretion for AGN (e.g., Fabian 1979, Rees 1984).

Among various types of AGN, only Seyfert galaxies and BL Lac objects are well studied for short time scale X-ray variability. This is partly due to their brightness in the X-ray band. Nandra et al. (1997) presented a systematic analysis the variability of X-ray flux for a sample of broad lined Seyfert galaxies observed by ASCA and found that the X-ray variability amplitude is well anti-correlated with the luminosity. Leighly (1999) demonstrated that a subclass of Seyfert galaxies called Narrow Line Seyfert 1 galaxies (NLS1s<sup>5</sup>, Osterbrock & Page 1985, Goodrich 1989) also follows an anti-correlation of amplitudes with luminosities, but for a given X-ray luminosity, NLS1s shows much larger variability amplitudes. This finding confirms the suspicion, based on the studies of individual objects, that NLS1s are more variable than normal Seyfert galaxies. Example of large variations can be found in literature

(e.g., Boller, Brandt & Fink 1996, Forster & Halpern 1996, Otani, Kii & Miya 1996).

PKS 0558-504 ( $z=0.137$ ,  $m_B=14.97$ ) is one of the rare radio-loud NLS1 type objects. Remillard et al. (1992) reported the detection of a rapid flare, in which the X-ray flux increased by 67% in 3 minutes, using the Ginga Satellite and suggested that the X-ray emission is enhanced by relativistic beaming. However, lack of imaging capacity of the Ginga makes this result somewhat questionable, as the flare might be due to a neighboring source. Recently, Gliozzi et al. (2000) observed this object with the ROSAT HRI in the soft X-ray band, they found also strong persistent variations in the soft X-ray band. But the  $\Delta L/\Delta t$  is considerably smaller than that reported by Remillard et al. (1992). In this paper, we report the detection of a rapid energetic flare in this object with imaging detectors.

## 2. OBSERVATION AND DATA REDUCTION

PKS 0558-504 was observed with ASCA (Tanaka et al. 1994) on January 31, 2000, with an effective exposure time of 37.4 ksec. The Solid-state Imaging Spectrometer (SIS) was operated in mixing faint and Bright 1-CCD mode, and the Gas Imaging Spectrometer (GIS) on pulse height mode. For the SIS, the faint mode data were converted into bright ones and combined with the bright data. The data reduction was performed in the standard way by using the FTOOLS (v4.2). Hot and flickering pixels were removed from the SIS data. To check the reliability of the scientific results, we have chosen both the strict data screening criteria and standard ones (see The ASCA Data Reduction Guide, version 2). The two yields consistent results, particularly on the flare profile. Since the standard one yields slightly better statistics in the X-ray spectrum,

<sup>1</sup>Center for Astrophysics, University of Science & Technology of China, Hefei, Anhui 230026, China (Email: twang@ustc.edu.cn)

<sup>2</sup>Space Utilization Research Program, NASDA, 2-1-1, Sengen, Tsukuba-city, Ibaraki 305-8505, Japan

<sup>3</sup>Department of Physics, Faculty of Science, Kyoto University, Sakyo-ku, Kyoto 606-8502, Japan

<sup>4</sup>The Institute of Physical and Chemical Research (RIKEN), 2-1, Hirosawa, Wako, Saitama, 351-0198, Japan

<sup>5</sup>We do not distinguish NLS1 and narrow line quasar, and call them simply NLS1

we will present it below. After standard screening, the net exposure times are 37.4 ks and 25.9 ksec for the GIS and SIS detectors, respectively.

The source counts were extracted from a circular region of 3.5 and 5.0 arcmin radius for SIS and GIS, respectively. The background counts were estimated from the off-source region at the same off-axis angle with same area for each of GIS detectors, and from the source subtracted region of the same chip of CCD for each of the SIS detectors. The background accounts for about 5 percent of total counts both for the SIS and GIS. The average net source count rates, after correcting for the background, are  $0.470 \pm 0.003$ ,  $0.598 \pm 0.004$ ,  $1.009 \pm 0.007$  and  $0.820 \pm 0.005$  cts sec<sup>-1</sup> for GIS2, GIS3, SIS0 and SIS1, respectively.

Light curves were extracted for the source and background for each detector. For both GIS detectors, the background count rate is nearly constant during the observation, therefore, an average count rate is used to estimate the background level. For the SIS detectors, the extracted background rate seems correlated with the source due to the contamination of the AGN. Therefore, it is only an upper limit to the true background, and is used only for spectral analysis. Since smaller extraction radii in the real sky are used for SIS detectors, the fraction of background light, thus, is estimated to be smaller than in the GIS case. We will ignore the background contribution to the SIS count-rate during the light curve analysis.

The X-ray spectra were rebinned to at least 25 counts per each bin. For the SIS spectrum, the response matrices appropriate for the date of the observation (thus accounting for decline of the energy resolution as a function of time) were made using the script *sisrmg*. For the GIS spectrum, the 1994 response matrices (*gis2v4\_0.rm* and *gis3v4\_0.rm*) were adopted. Ancillary response files were made for each detector using *ascaarf*. The ASCA data preparation and the spectral analysis were performed using version 1.4 of the XSELECT package and version 10.01 of XSPEC.

### 3. SPECTRAL AND TEMPORAL ANALYSIS

#### 3.1. The Spectral Properties

Since the efficiency of SIS detectors has decreased due to the radiation damage and the current calibration files does not account for this, SIS spectra only above 0.8 keV are used. The GIS spectra below 0.8 keV are not well calibrated and will be not used in the spectral fit. The X-ray spectra in the full ASCA band cannot be adequately described by an absorbed power-law with a  $\chi^2/d.o.f = 1058/924$ , which is accepted at a probability of only  $1 \times 10^{-3}$ . There are systematic deviations at low energies. In addition the fitted column density  $(2.4 \pm 1.2 \times 10^{20} \text{ cm}^{-2})^6$  is significantly lower than the galactic value ( $4.5 \times 10^{20} \text{ cm}^{-2}$ ).

In order to see if this is due to soft X-ray excess, which was noticed in the Ginga spectrum (Remillard et al. 1992), we initially fitted the spectrum above 2.0 keV. Single power-law with the Galactic absorption provides a good fit to the joint GIS and SIS spectra ( $\chi^2/d.o.f = 631/636$ ). The best fitted photon index ( $\Gamma = 2.20^{+0.02}_{-0.04}$ ) is slightly flatter than the previous fit ( $\Gamma = 2.25^{+0.02}_{-0.03}$ ). This spectral index matches well the one obtained by Leighly et

al. (1999) for 1997 observation, suggesting no significant variation in the spectral index between the two observations. Extrapolating this fit to low energies shows excesses in the soft X-ray band (Fig. 1), particularly below 1.2 keV. The excess is larger in the GIS spectra than in the SIS ones, and also larger in the SIS0 than in the SIS1, possibly indicating the decreasing efficiency of SIS already evident in the energies just below 1.2 keV. If the soft excesses are modeled with black body emission, the best fit yields a  $kT = 0.22 \pm 0.02$  keV and a normalization  $3.4^{+1.3}_{-1.0} \times 10^{-5}$ . The latter corresponds to a flux in 0.8-2 keV flux of  $2.1 \times 10^{-12} \text{ ergs sec}^{-1} \text{ cm}^{-2}$ . Though this fit is better than the single power-law fit by  $\Delta\chi^2 = 31$ , however, it is still statistically acceptable only at 1% probability ( $\chi^2/d.o.f = 1027/923$ ). After carefully examining the residuals, we find that counts in the SIS detector is significantly lower than these of GIS at energy below 1.15 keV. This most likely is due to the degeneration of the SIS sensitivity at low energies. In fact, the fit is acceptable (926/894,  $P_r = 0.22$ ) when the SIS data below 1.2 keV were ignored. This fit yields an  $kT = 0.13^{+0.03}_{-0.02}$  keV and a normalization  $1.50^{+1.10}_{-0.53} \times 10^{-4}$ . The photon index for this fit is  $2.22^{+0.02}_{-0.03}$ , similar to that derived for fitting 2-10 keV spectrum.

Recently, O'Brien et al. (2000) found that the soft excess extends up to 3 keV from their much higher quality XMM spectrum and can be modeled as multiple temperature blackbody emission. The spectral slope of the power law component is 0.9, fully consistent with those found in other Seyfert 1 galaxies. The steep hard X-ray component found in the ASCA spectrum could be due to the contamination of the spectroscopically unresolved soft X-ray excess in the ASCA 2-10 keV band.

No iron K line is detectable with the ASCA data. An upper limit of equivalent width for a narrow Gaussian line at 5.5 or 5.7 keV (6.4 and 6.7 keV in the source rest frame) is 40 eV, consistent with XMM result (O'Brien et al 2000).

#### 3.2. Temporal Properties

Fig. 2a shows the combined GIS and SIS light curves for the count rates in 0.8-10 keV and 0.6-10 keV bands, respectively. A large energetic flare started shortly after the observation. The count rate increased from  $0.54 \pm 0.02$  cts/s to  $1.10 \pm 0.04$  cts/s in about 2000 sec and then decreased to  $0.50 \pm 0.02$  cts/s in about 3500 sec. Since there are observation gaps in between, the real variations might be even faster.

We have examined possible contamination sources. The background count rates are stable and at only a few percent level of the source count rates during the observation. Concerning the impact of particle background, we have applied strict screening criteria to the GIS data (refer to The ASCA Data Reduction Guide, version 2), the flare structure remained. The source position measured in the ASCA GIS image is 05 59 41.1: -50 27 24.1 (equinox 2000), which has an offset of  $\Delta\alpha = 1.58'$  and  $\Delta\delta = 0.39'$  from the NED position of PKS 0558-504. However, after correcting for a temperature dependent deviation of the attitude solution (Gotthelf et al. 2000), the ASCA position deviates from the NED one of about  $13''$ , which is within the 90% error circle ( $24''$ ) of the GIS. We also noted that the image ex-

<sup>6</sup>Uncertainties are given at 90% confidence level for one interesting parameter for all the spectral parameters given in this section

tracted for the events collected during the flare phase has a position 09 59 40.4 -50 27 16.8, which is only 11'' away from the position of the source in the total observation for the GIS. This analysis sets that any confusing source should be within 20'' of the PKS 0558-504. The analysis of the SIS data gives a similar conclusion, but detailed number is not given here since our main analysis below concentrates on the GIS curve.

The SIS curve is similar to the GIS one. The flare is also clearly present in the SIS data. Due to different screening criteria applied to the SIS and GIS, the SIS data just before the peak of flare are not available. Thus, the flare profile is less well defined than in the GIS curve.

The flare is shown with increased time resolution (GIS 64-s bins) in Fig. 2b. Clearly, the source shows variability on short time scales of 10<sup>2</sup>s. A  $\chi^2$  test on the constancy of count-rate for the second group of the data in Fig 2b gives a  $\chi^2/d.o.f=45.6/21$ , which is at a probability  $P_r=0.002$  by chance. The pre-flare has a mean count rate of  $0.53 \pm 0.02$  cts/s for an interval of 650 seconds. Unfortunately, there is a 1000 sec gap just before the on-set of the flare. Nevertheless, the flare rose very fast. The count rate increased from  $0.82 \pm 0.05$  cts/s (average over three bins) to the peak count rate  $1.14 \pm 0.05$  cts/s (three bins average) in less than 128 sec. The statistical significance of this change is about 4.5  $\sigma$ . This gives a rate of change in the count-rate  $\Delta CR/\Delta t \simeq (2.5 \pm 0.6) 10^{-3}$  cts s<sup>-2</sup>. A more subjective estimation of the rate by linear fit to the rising part of the curve (first 7 points in the second group of data, see Fig 2b). This gives a rate  $\Delta CR/\Delta t \simeq (1.14 \pm 0.28)$  cts s<sup>-2</sup>, a factor of two lower than the one from direct visual inspection. We will quote the latter more conserved number in later discussion. The source was then dimming with possible flicker till the end of this orbit. The presence of the second peak probably is also real since it appears in the SIS curve as well. The flux returns to the pre-flare level at the beginning of the next orbit observation.

We define two bands based on the spectral range of the soft X-ray excess (see §3.1). The energy ranges are 0.8-2.0, 2.0-10 keV for soft and hard bands for GIS data. The soft band extends to 0.5 keV for the SIS data since there is a substantial fraction of counts in the energy range 0.5-0.8 keV. The light curves for these two bands were extracted in order to examine possible spectral variations during the flare. The flare is seen in both bands. However, it shows larger amplitude and decays faster in the hard band than in the soft one. The ratios of the count rate for the flare peak to the pre-flare are  $1.70 \pm 0.13$  and  $2.13 \pm 0.17$  for the soft and hard bands, respectively. There is no significant decrease in the count rate of the soft band during the flare orbit ( $\chi^2/d.o.f = 3.4/3$ ,  $P_r > 0.3$  for a constant count rate in the last 1024 seconds during the flare orbit), in contrast to the clear rising and fading in the curves of hard band ( $\chi^2/d.o.f = 15.0/3$ ,  $P_r \simeq 0.002$  for the same  $\chi^2$  test) (Fig 3).

We examine whether there is a correlation between the hardness ratio and the total count-rate and whether the flare follows the same correlation. The hardness ratio is the ratio of count rates in the 2-10keV band and in the 0.8-2.0 keV band. In order to achieve a reasonable S/N ratio for each bin, we use a 1024 sec binning light curves. The hardness ratio is weakly anti-correlated with the total count-rate for normal variations. A Spearman rank

correlation analysis gives a correlation coefficient of  $r = -0.371$  ( $n=62$ ) for which the probability for null hypothesis is  $P_r=0.3\%$  for the GIS data (we have ignored these data points with uncertainty in the ratio larger than 0.15). In figure 4, we add the hardness ratios for the flare phase, which is binned with 512 seconds binning. The flare is distinguished itself from others for having large hardness ratio and large count-rate (Fig. 4). In fact, the first three data points of the flare phase have hardness ratio among the largest. And the last data point of the flare returns to the average hardness ratio. If the spectrum during the flare is a power-law, the power-law indices is about 1.9 for the first three points of the flare and 2.2 for the last point of the flare (Fig. 4). It is not clear that if the decreasing hardness ratio indicates a time delay between the two bands. Cross correlation analysis does not found any definite delays between the soft X-rays and the hard X-rays.

Since the first three data points during the flare imply a spectral index of 1.9 (see Fig. 4), which is significantly harder than the mean spectral index in the 2-10 keV band, the change in the hardness ratio cannot be explained with the change of relative contribution of the soft excess alone. The spectrum in the 2-10 keV band must also have changed. However, if the hard X-ray spectrum is as flat as  $\Gamma = 1.9$ , suggested by the XMM observation (O'Brien et al. 2000), then during the large flare, the X-ray emission is dominated by the hard power-law.

#### 4. DISCUSSION

We observed a rapid flare in the PKS 0558-504, during which the X-ray count rate increased by a factor of nearly two in 33 minutes, and possibly 40% in as short as two minutes. This result independently confirms the existence of a rapid flare in this object obtained by Ginga (Remillard et al., 1992) and further suggests that the flare is repetitive. ROSAT HRI observation also found that the object is highly variable in the soft X-ray band, but no such clearly rapid flare event was seen (Gliozzi et al. 2000). This might be due to the relatively flat spectrum during the flare phase (a much lower amplitude in the soft X-ray band) and/or to the low photon collecting area of the ROSAT HRI or it does not happen to catch a flare. Neither the ASCA observation in 1999 nor the XMM observation in 2000 (Gliozzi et al 2001) detected a rapid flare. The total exposure time, by summing up those of Ginga, ASCA and XMM observations, is about 150 ks, in which rapid flares were detected twice. This suggests that rapid flares occur not in-frequently in this object.

The fastest variation during the rise of flare phase suggests a rate of change in the count rate  $\Delta CR/\Delta t = (1.14 \pm 0.28) 10^{-3}$  cts s<sup>-2</sup> in a linear fit. Assuming the X-ray spectrum can be described by a power-law, the flare has a spectrum with a photon index of  $\simeq 1.9$  from its hardness ratio, the rate of change in the count-rate yields a  $\Delta L/\Delta t = (1.8 \pm 0.4) 10^{42}$  ergs s<sup>-2</sup> in the 0.8-10 keV band (assuming  $H_0 = 75$  and  $q_0 = 0.5$ ) if the X-ray emits isotropically. Note this value is similar to the one obtained during the Ginga observation. Since the flare spectrum must be not limited in the 0.8 to 10 keV band, the actual  $\Delta L/\Delta t$  should be larger. If the hard X-ray spectrum extends to energy as high as 100 keV, then the flare luminosity will be a factor of 2 higher. Notice that there is a limit on  $\Delta L/\Delta t \leq 2 10^{42} \eta$  ergs sec<sup>-2</sup>, where  $\eta$  is the efficiency of

converting matter to radiation, for spherically distributed plasma whose opacity is dominated by Thomson scattering (e.g., Guilbert, Fabian, & Rees 1993). The  $\Delta L/\Delta t$  given above yields an efficiency of  $\eta = 0.9 \pm 0.2$ , which exceeds the limit for accretion even onto a Kerr hole. This was interpreted as an evidence for the relativistic beaming in this object by Remillard et al. (1991).

#### 4.1. A Flare from Relativistic Jets ?

Since PKS 0558-504 is a radio-loud quasar, we will first examine the possibility that the flare is produced in relativistic radio jets. There are evidences that the X-ray is dominated by the emission from relativistic jets in radio loud quasars (e.g., Worrall & Wilkes 1990). Relativistic beaming is expected naturally in this case if the jet beams towards us. We noticed that the broad band optical/UV to X-ray spectrum is flat with a spectral index  $\alpha = (1.1-1.3)$ , in the range for radio-loud quasars (Brinkmann, Yuan & Siebert 1997). Lack of a detectable Fe K $\alpha$  line is also consistent with the X-ray observations of other radio loud quasars. However, the X-ray spectrum of PKS 0558-504 in the 2-10 keV band is much steeper than that of a typical radio loud quasar. It resembles those of High energy peaked BL Lac (HBL) objects, in which the X-ray spectrum is believed to be the tail of the synchrotron emission of the relativistic jets (e.g., Kubo et al. 1998). Furthermore, we notice that HBL objects also show a loop structure on the plane of hardness ratio versus count rate during flares, possibly due to the synchrotron cooling of electrons (e.g., Kataoka et al. 2000). Since the jet in a BL Lac object is thought to beam towards the observer, this meets the requirement of relativistic boosting. Even for BL Lac objects, such fast ( $\leq 10^3$ s) flares were only reported in a few cases (Feigelson et al. 1986; Catanese & Sambrana 2000).

But PKS 0558-504 is not BL Lac object. It has prominent emission lines, instead of weak or non-detectable emission lines for a BL-Lac object. In addition, PKS 0558-504 shows a steep radio spectrum with a 2.7 GHz to 5 GHz spectral index of 0.88 (Wright & Otrupcek 1990, Gregory, Varasour, Scott, & Condon 1994, and Wright, Friffith, Burker & Ekers 1994), in contrary to the flat radio spectra of BL-Lac objects. And finally, the fact that the continuum of PKS 0558-504 is dominated by a big blue bump extending to the soft X-ray band suggests that the non-thermal emission from jets unlikely overwhelms the nucleus emission by a large factor even in X-ray band (O'Brien et al. 2000).

This does not rule out the possibility that the X-ray flare is induced by a relativistic jet while the emission is from the nucleus in the normal state. The fact that the X-ray spectrum during the flare phase tends to be flatter than the average spectrum is consistent with it being from a distinct component. If the nucleus component has a flux similar to the average value, half of the count rate during the flare must come from the nucleus component since count rate during the flare is a factor two of the normal state. Then the flare component could be as flat as a power-law with an index 1.6.

#### 4.2. A Magnetic Flare?

Given that there is no evidence of associating the flare with radio jets in PKS 0558-504, we consider the possibility that it arises from the nucleus. Rapid variations in the

X-ray band are common even in the radio quiet NLS1s, where no relativistic radio jet has been observed. Some extreme variations in objects such as PHL 1092, IRAS 13224-3809, also suggest a radiative efficiency larger than those setting by accretion matter onto Schwarzschild black holes (e.g., Forster & Halpern 1996, Boller, Brandt & Fink 1996). As discussed by Guilbert, Fabian & Rees (1983) that either non-spherical geometry or continuous acceleration of electrons can generate a large effective radiative efficiency. Particularly interesting is a magnetic corona model, in which particles in the corona are continuously heated up by magnetic reconnection and up-scatter the soft photons from the accretion disk into X-rays. Since the magnetic field does not contribute to the scattering opacity, this will raise the effective efficiency. If the energy is pre-stored in the magnetic field co-region with the emission plasma, the effective efficiency can be as large as  $\eta \leq B^2/(8\pi\rho_0 c^2)$ , where  $B$  is the strength of magnetic field,  $\rho_0$  the mass density of the corona region. When the magnetic energy density approaches to that of the rest mass, the  $\eta$  is order of 1. In this model, the X-ray spectral index is a function of the particle temperature and the optical depth of the corona. The temperature is determined by the balance of the heating and cooling rate since the Compton cooling is very effective for hot electrons in NLS1s as estimated below.

The electron energy loss rate is

$$\frac{dE}{dt} = n_e \int \frac{U_\nu}{h\nu} c \sigma_T \frac{4kT - h\nu}{m_e c^2} h\nu d\nu \quad (1)$$

where  $U_\nu$  is the specific radiation energy density at frequency  $\nu$ ,  $\sigma_T$  the Thomson cross section,  $m_e$  the rest mass of an electron, and  $T$  is the electron temperature. If the average photon energy is much smaller than the thermal energy of hot electrons, then we can ignore the process of transferring photon energy to an electron. One can easily get a cooling time scale for hot electrons:

$$\tau_c \simeq \frac{3\pi}{2} \frac{m_e c^2}{\sigma_T} \frac{r^2}{L} = 58 L_{45}^{-1} r_{14}^2 \text{sec} \quad (2)$$

Where  $L$  is the luminosity in the UV and soft X-ray bands,  $r$  the size of the continuum emission region,  $L_{45} = L/(10^{45} \text{ ergs/s})$  and  $r_{14} = r/(10^{14} \text{ cm})$ .

For typical luminosity and size of emission region, this time-scale is rather short in comparison with the typical flux variation time scale. Therefore, if the hard X-ray emission is produced by the Compton scattering process, the fading time (order of  $10^3$  sec) seems irrelevant to the electron cooling process, but more likely due to variations of electron heating rate, e.g., magnetic reconnection rate or even the coupling time of electrons with ions.

If a flare is energized by magnetic reconnection, then the total energy stored in the magnetic field  $(B^2/8\pi)l^3$  must be not less than the total energy emitted during the flare  $(\Delta L \Delta t)$ , where  $l$  is the scale of the magnetic field,  $\Delta L$  and  $\Delta t$  are the luminosity and the duration of the flare. When an anomalous resistivity is introduced, the magnetic reconnection takes place and it spreads at a speed of Alfvén velocity,  $v_A = (B^2/4\pi\rho)^{1/2}$ . The global magnetic field dissipation time should be not shorter than  $l/v_A$ . Notice that converting a significant power into X-rays needs

a Thomson optical depth  $\tau_T$  of orders of 1. Putting all these together, one yields the time scale of variability:

$$\Delta t \geq 4 \cdot 10^3 \Delta L_{45}^{1/5} B_4^{-8/5} \tau_T^{3/5} \text{ sec} \quad (3)$$

where  $B_4 = B/10^4$  Gauss,  $\Delta L_{45} = \Delta L/(10^{45} \text{ ergs/s})$ .  $\Delta t$  is sensitive to magnetic field strength, but only weakly depends on the luminosity. For the fastest variation during the rising phase of the flare,  $\Delta L = 5 \times 10^{44} \text{ ergs/s}$  in  $\Delta t = 280 \text{ sec}$  (using the linear fit result), one yields  $B \geq 5 \times 10^4 \tau_T^{3/8}$  Gauss for the flare region. If part of the energy dissipated via magnetic reconnection is converted into kinetic energy, causing bulk motion of the flaring material (Beloborodov 1999). The bulk motion would boost the apparent variability if it is towards the observer. However, the flare material is only mildly relativistic, as estimated by Beloborodov (1999), this would not seriously affect the magnetic field given above.

The strength of the magnetic field in an accretion disk is in principle limited by equipartition with the disk pressure. Stronger magnetic field will rise buoyantly from the accretion disk, leading to a magnetically confined corona (Galeev, Rosner & Vaiana 1979). Mineshige et al. (2000) argued that the magnetic field is large in the NLS1s due to large pressure caused by the trapped photons in the inner region (radiation pressure dominated) of a slim disk. By requiring  $P_{\text{mag}} \leq P_{\text{disc}} \simeq P_{\text{rad}} = aT^3/3$ , one can estimate the temperature of the disk of the region that produced the flare. This gives a  $kT_{\text{disk}} \geq 38 \text{ eV}$ , which is somewhat lower than that of the lowest temperature component in O'Brien et al.'s multiple black body model derived from the broad band XMM spectrum. This perhaps explains why a rapid energetic flare could only observed in NLS1s with extremely steep soft X-ray.

#### 4.3. The Black Hole Masses in Radio Loud NLS1s

There is growing evidence for more massive black holes (BH) in radio-loud quasars than in radio quiet ones. By assuming the line emitting gas is virialized, Laor (2000) derived BH masses of the radio loud QSOs above  $10^9 M_\odot$ , significantly larger than in radio quiet QSOs. This result is in line with the recent identified correlation between the mass of the central BH and that of the bulge (Magorrian et al. 1998, Gebhard et al. 2000, Ferrarese & Merritt 2000), together with the fact that the radio loud objects are hosted by elliptical galaxies. It is not understood how the jet formation is related to the mass of the central BH in AGN, the galactic BH binaries also show super-luminal radio jets but their typical mass is around  $10 M_\odot$ <sup>7</sup>. McLure et al. (1999) found that both luminous radio-loud and radio quiet quasars reside in elliptical galaxies, suggested massive BH for both type QSOs.

On the other hand, it was suggested that the formation of jets might be related to the low accretion rate, such as in advection dominated accretion flow (e.g. Rees, Begelman, Blandford & Phinney 1982, Blandford & Begelman 1999) and/or with the spin of the BH (Blandford & Znajek 1977). It is worthy to mention that the radio emission from the BH X-ray binaries also appear to be strong in the low state (Fender 2000), while it is suppressed in the high state.

However, evidence shows that the PKS 0558-504 possesses a low mass BH and high accretion rate. The  $H\beta$  width of this object is around  $1250 \text{ km s}^{-1}$  (Corbin 1997) and the optical continuum luminosity  $\nu L\nu(5100\text{\AA}) \simeq 2.2 \cdot 10^{45} \text{ erg s}^{-1}$  from the V magnitude and corrected for the Galactic reddening (Corbin & Smith 2000). By adopting the empirical Broad Line Region (BLR) size versus optical luminosity relation,  $R_{\text{BLR}} \simeq 18.65[\lambda L\lambda(5100\text{\AA})/10^{44} \text{ ergs s}^{-1}]^{0.7}$  (Kaspi et al. 2000), and further assuming that the broad line region is virialized, we can derive a mass of central BH of  $4.5 \times 10^7$  solar mass. With this BH mass, the object is emitting at super-Eddington luminosity. Note the mass of the central BH is far less than those seen in the radio loud quasars in the PG sample (Laor 2000), which was inferred with the same method. We wish to point that the V-magnitude of PKS 0558-504 is 14.97 and its B-V, U-B values similar to those of 3C 273. If it were in the north sky, it would be selected as a PG QSO as well.

There are a number of uncertainties in the above estimation of the mass. We have used the empirical  $R_{\text{BLR}} - L_{\text{opt}}$  relation. The BLR is photo-ionized by far/extreme UV photons, the size may scale more adequately with the ionizing continuum than with the optical luminosity. Since PKS 0558-504 shows very big blue bump as detected by XMM in optical-UV and broad band X-ray (O'Brien et al. 2000), it has more ionizing flux than a typical QSO with similar optical luminosity, thus a larger BLR. To give the order of magnitude of this correction, we estimate an optical to UV spectral slope  $\alpha \simeq 0.1$ , which is 0.4 lower than typical QSO value. If this spectrum extends to the Lyman limit, there is a factor of 2 more flux at this  $912\text{\AA}$  than for typical QSO spectrum. This will only increases the mass of BH by a factor of 1.5, which is still far less than the masses of BHs in radio loud PG QSOs. Since by this way, the increase of ionizing photon flux also raises the bolometric luminosity, this would not lower the fraction accretion rate. Another concern is that the BLR is in a flat structure, so that the velocity depends strongly on the inclination of the system. There is evidence for the anisotropy of BLR velocity in radio loud AGNs, and the  $H\beta$  line width is found to be anti-correlated with the core dominance of the radio source. There is no such radio data for the PKS 0558-504, so it remains possible that we might see a flat BLR from top in this object and the mass of central BH was under-estimated. However, the core dominated radio source usually display flat spectrum, instead of the steep radio spectrum in these objects (see §4.1). High resolution radio observation, however, is necessary to address this.

The other two radio loud NLS1s (RGB J0044+193 and RX J0134.2-4258) have even lower BH masses and higher accretion rates. Using the same method, we find that the BH masses are  $1.6 \times 10^7$  and  $10^7 M_\odot$  for RGB J0044+193 and RX J0134.2-4258, respectively. These two objects show the same characteristics in the SED as PKS 0558-504: a very big blue bump indicated by its flat optical to UV continuum and huge soft X-ray excess, steep radio spectrum, and weak iron K line (Siebert et al. 1999, Grupe et al. 2000). The mass of RGB J0044+193 can be an order of magnitude larger if the BLR size scales with the luminosity of ionizing continuum instead of the lumi-

<sup>7</sup>They are formally radio-quiet according to the definition of radio loudness  $R = \log(f_{5\text{GHz}}/f_{\text{opt}})$  in AGN.

osity at  $5100\text{\AA}$  and if its extremely steep continuum in the optical spectrum ( $\alpha_{\text{opt}} \simeq -3.1$ , Siebert et al. 1999) extends into far UV. However, we notice that the equivalent width of  $\text{H}\beta$  is normal in this object, suggesting such kind of correction is not adequate.

If above mass estimation is correct, the existence of radio-loud NLS1s suggests that neither large mass of the BH nor a low accretion rate is necessary for the formation of a powerful radio jet. So what else factor is relevant, spin of a BH or the environment of the galactic nuclei? If a jet is powered by the spin energy of the BH through Blandford & Znajek (1977) mechanism, both rapid spin of the BH and a strong magnetic field are required for the formation of powerful radio jets. Formation of a rapidly spinning BH in NLS1s can be found in various schemes: a massive hole is formed through collapsing of a rotating gas clouds, through accreting material by a seeded small hole and by merging of small holes. In particular, the hole spins up very fast in NLS1s as they are thought to accrete at close to or even super-Eddington rate. It can easily reach the equilibrium between the spin-up by accretion and the spin-down by the Blandford-Znajek mechanism (Moderski, Sikora & Lasota 1998) unless the NLS1s phase is extremely short (less than a few  $10^7$  years). Strong magnetic field can be either created by the dynamo in the accretion disk or amplified by compressing the convected magnetic field frozen in the accreted material. It remains unexpected that radio loud NLS1s are so rare.

Alternatively, it was suggested that the observed radio jets are related not only with the center engine but also with the environment of the nuclei that provide the confinement of the jets. If this is indeed the case, the host galaxies of the RL NLS1s should be also a massive elliptical galaxies. We speculate that they deviate from the relation between mass of BH and that of bulge because the BH is still in the rapid growth phase. We have no data on the bulge masses of these three NLS1s. Nelson & Whittle (1996) suggest that  $[\text{OIII}] \lambda 5007$  width is a good indicator of stellar velocity dispersion in elliptical galaxies and spiral bulges. The  $[\text{OIII}]$  widths are 670 and  $750 \text{ km s}^{-1}$  for

RX J0134.2-4258 and RGB J0044+193 (Siebert et al 1999; Grupe et al. 2000), respectively, which correspond to stellar velocity dispersions of 285 and  $319 \text{ km s}^{-1}$ , indicating of massive spheroidal component in both galaxies. This would give BH masses of about  $4\text{--}6 \cdot 10^8 M_{\odot}$  in these two objects if they were followed BH mass and stellar velocity dispersion relation (Fig. 1 of Nelson 2000). These masses are one order of magnitude larger than the BH masses estimated from the BLR-kinematics method, consistent with our guess. The  $[\text{OIII}]$  is extremely weak in PKS 0558-504 and its has not been given by Corbin (1997), but seems also relative broad. However, a direct measurement of the stellar velocity dispersion in those objects is needed before any firm conclusion can be drawn.

To summarize, we find that the rapid flare observed in PKS 0558-504 requires an effective radiative efficiency of close to one. This can be explained either by associating the flare with the relativistic radio jets or magnetic heated corona above an accretion disk. Future simultaneous monitor of this object in radio and X-ray bands would be crucial in discrimination the two possibility. We showed that a magnetic field of strength of at least a few  $10^4$  Gauss is required in the latter case. Future observation with a large photon collecting areas detector, such as MAXI program, will allow un-interrupt monitoring the detail spectral evolution of the flare, yielding stringent constraints on the models. We found that the masses in three RL NLS1s are much lower than that for radio loud quasars, which may suggest that the black holes in narrow line NLS1 are still in the phase of rapid growth.

The authors thank the ASCA team for successfully carrying out this observation. TW wishes to thank Youjun Lu for many useful comments on an early version of this draft. TW acknowledges the financial support of Chinese NSF through NSF-19925313 and of Chinese Science and Technology Ministry. This research has made use of the NASA/IPAC Extragalactic Database (NED) which is operated by the Jet Propulsion Laboratory, California Institute of Technology, under contract with NASA.

## REFERENCES

- Barr, P. & Mushotzky, R.F. 1986, *Nature*, 320, 421  
 Beloborodov, A.M., 1999, *ApJ*, 510, L123  
 Blandford R.D., & Znajek R.L., 1977, *MNRAS*, 179, 433  
 Boller, Th., Brandt, W.N., & Fink H.H. 1996, *A&A*, 305, 53  
 Brinkmann W., Yuan W, Siebert J., 1997, *A&A*, 319, 413  
 Catanese, M., & Sambruna, R.M. 2000, *ApJ*, 534, L39  
 Corbin, M.R. 1997, *ApJS*, 113, 245  
 Corbin, M.R. 2000, *ApJ*, 532, 136  
 Fabian, A.C. 1979, *Proc. Roy. Soc. London A*, 366, 449  
 Feigelson, E., et al. 1986, *ApJ*, 302, 337  
 Ferrarese L. & Merritt D. 2000, *ApJ*, 539, L9  
 Fender, R.P., 2000, *MNRAS*, in press (astro-ph/0008447)  
 Forster K., & Halpern, J.P. 1996, *ApJ* 468, 565  
 Galeev, A.A., Rosner, R. & Vaiana, G.S., 1979, *ApJ*, 229, 318  
 Gebhardt, K., et al., 2000, *ApJ*, 539, 13  
 Giommi, P., et al., 1999, *A&A*, 351, 59  
 Gliozzi, M., Boller, Th., Brinkmann W., Brandt, W.N. 2000, *A&A*, 356, L17  
 Gliozzi, M., Brinkmann, W., O'Brien, P.T., Reeves, J.N., Pounds, K.A., Trifoglio, M. & Gianotti, F. 2001, *A&A*, 365, L128  
 Goodrich R.W. 1989, *ApJ*, 342, 224  
 Gotthelf E.V., Ueda Y., Fujimoto R., Kii T. & Yamaoka K., 2000, *ApJ*, 543, 417  
 Guilbert P.W., Fabian, A.C., & Rees, M.J. 1983, *MNRAS*, 205, 593  
 Gregory, P.C., Varasour, J.D., Scott, W.K., & Condon, J.J. 1994, *ApJS*, 90, 173  
 Grupe D., Leighly K.M., Thomas H.C., Laurent-Muehleisen S.A. 2000, *A&A*, 356, 11  
 Kaspi, S., Smith, P. S., Netzer, H., Maoz, D., Jannuzi, B. T., Giveon, U., 2000, *ApJ*, 533, 631  
 Kataoka, J., Takahashi T., Makino F., Inoue, S., Madejski G.M., Tashiro, M., Urry C.M., Kubo, H. 2000, *ApJ*, 528, 243  
 Kubo H., et al., 1998, *ApJ*, 504, 693  
 Leighly, K., 1999a, *ApJS*, 125, 297  
 Leighly, K., 1999b, *ApJS*, 125, 317  
 Laor A., 2000, *ApJ*, 543, L111  
 Magorrian J., et al. 1998, *AJ*, 115, 2285  
 McHardy, I. M. 1989, *Proc.*, 23rd ESLAB Symp. eds. J. Hunt & B. Battrick (Paris:ESA) p. 499  
 McLure, R. J., Kukula, M. J., Dunlop, J. S., Baum, S. A., O'Dea, C. P., Hughes, D. H. 1999, *MNRAS*, 308, 377  
 Mineshige, S., Kawaguchi, T., Takeuchi, M., & Hayashida, K., 2000, *PASJ*, 52, 499  
 Moderski R., Sikora M., & Lasota J.P. 1998, *MNRAS*, 301, 142  
 Nandra K. et al. 1997, *ApJ*, 476, 70  
 Nelson C.H., Whittle, M., 1996, *ApJ*, 465, 96  
 Nelson C.H., 2000, *ApJ*, 544, L91  
 O'Brien, P.T., et al., 2001, *A&A*, 365, L122  
 Osterbrock, D.E., & Pagge R.W. 1985, *ApJ*, 297, 166  
 Otani, C., Kii, T., & Miya, K. 1996, in *Röntgenstrahlung from the Universe*, ed. H.U. Zimmermann, J.E. Trümper & H. Yorke (MPE Press, Garching), p. 491

- Rees M.J., Begelman M.C., Blandford R.D., & Phinney E.S. 1982, *Nature*, 295, 17
- Rees, M.J. 1984, *Ann. Rev. Astron. & Astrophys.*, 22, 471
- Remillard, R.A., Grossan, B., Bradt H.V., Ohashi T., Hayashida K., Makino F., & Tanaka Y. 1992, *Nature*, 350, 589
- Siebert J., Leighly K.M., Laurent-Muehleisen S.A., Brinkmann W., Boller Th. & Matsuoka M. 1999, *A&A*, 348, 678
- Worrall, D.M., & Wilkes, B.J. 1990, *ApJ*, 360, 396
- Wright, A., & Otrupcek, R., 1990, *Parkes Catalogue*, Australia Telescope Nation Facility.
- Wright, A.E., Griffith, M.R., Burkner, B.F., & Ekers 1994, *ApJS*, 91, 111

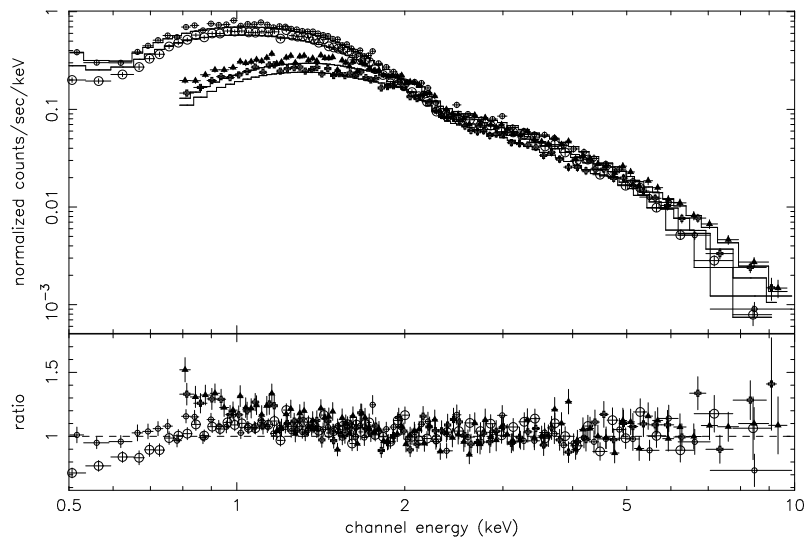


FIG. 1.— The ASCA spectra of PKS 0558-504 (upper panel) and the ratios of data to a best power-law fit to the 2-10 keV band data (low panel). The SIS0, SIS1 and GIS2 and GIS3 data are marked with small circles, large circles, crosses and triangles, respectively. Systematic excesses over the power-law are clearly present. The SIS spectrum is plotted to 0.5 keV for the purpose of illustrating the degeneration of the SIS efficiency.



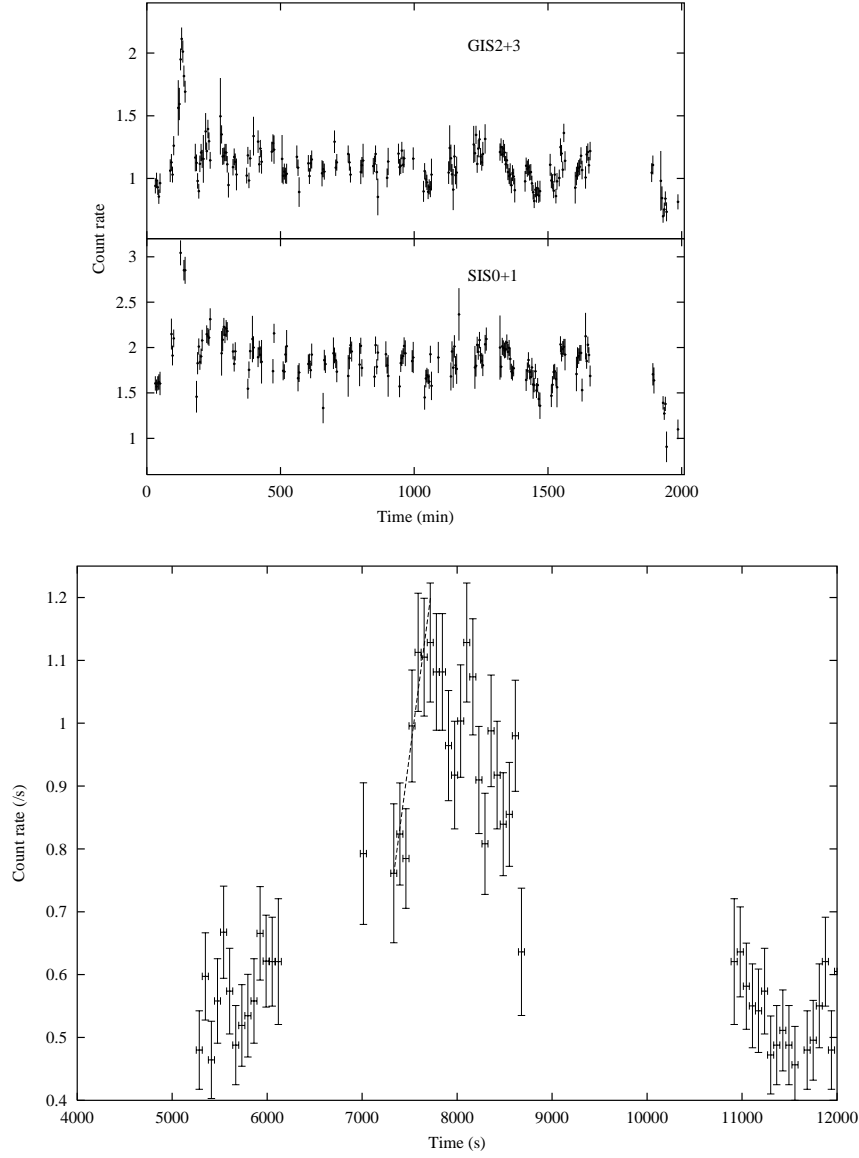


FIG. 2.— The ASCA SIS and GIS light curves for the PKS 0558-504 (Fig. 2a). The count rate is binned in 256 s bins, and the data from two SIS and two GIS detectors have been combined. The background count rate, which is about 5% of the total, has not been subtracted. The flare is clearly present in the both SIS and GIS data, and is shown in enlarged scale in the Fig. 2b for GIS data. A dashed line represents the linear fit of the steep rising part the light curve for estimation of the rate of change in the count rate.

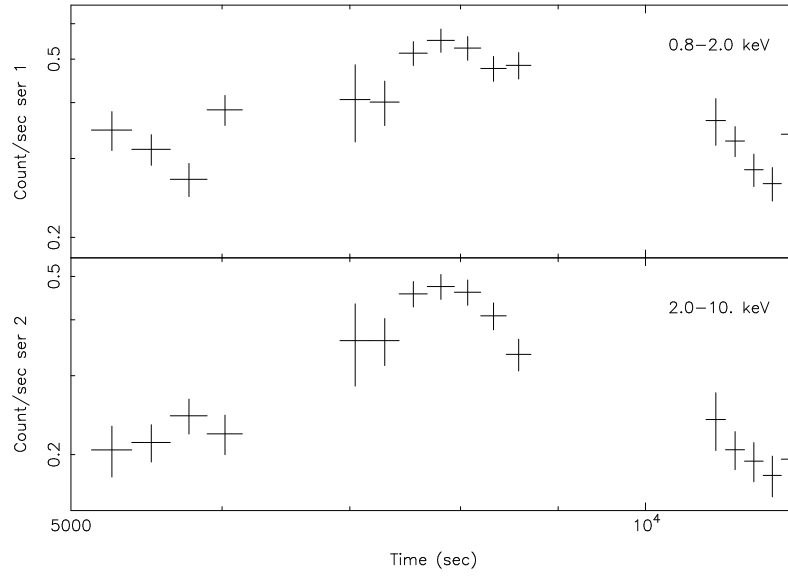


FIG. 3.— The hard and soft X-ray GIS light curves for the time period from pre-flare to post-flare. Notice that the soft band shows different flare profile with the hard one. The SIS curves show a similar character (not shown here).

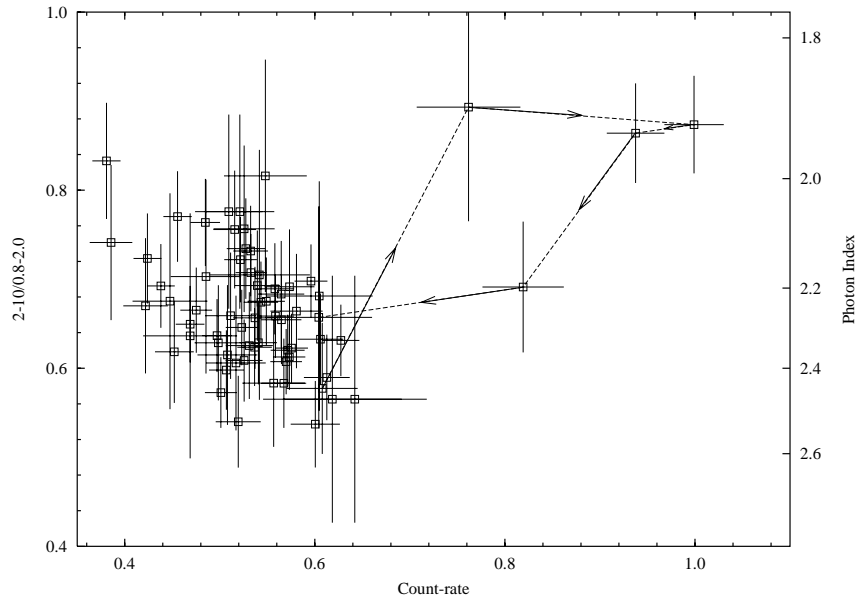


FIG. 4.— The plot of hardness ratio against the total count rate in the 0.8-10 keV band for the SIS data. The right y-axis also shows the corresponding photon index assuming a power-law spectrum. The data points during the flare and in the neighbor are connected with line and the arrows indicate the proceeding direction of the flare. Notice that the flare show a clockwise loop structure on the plot.